ORNL-5293

Substructures Developed During Creep and Cyclic Tests of Type 304 Stainless Steel (Heat 9T2796)

R. W. Swindeman
R. K. Bhargava
V. K. Sikka
J. Moteff

BLANK PAGE

Printed in the United States of America. Available from
National Technical Information Service
U.S. Department of Commerce
5285 Port Royal Road, Springfield, Virginia 22161
Price: Printed Copy $4.00; Microfiche $3.00

ORNL-5293
Distribution
Category - UC-79b, -h, -k

Contract No. W-7405-eng-26

METALS AND CERAMICS DIVISION

SUBSTRUCTURES DEVELOPED DURING CREEP AND CYCLIC TESTS OF TYPE 304 STAINLESS STEEL (HEAT 9T2796)

R. W. Swindeman

R. K. Bhargava

V. K. Sikka

J. Moteff

Date Published: September 1977

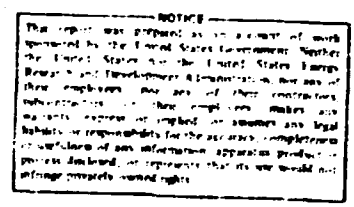

OAK RIDGE NATIONAL LABORATORY
Oak Ridge, Tennessee 37830
operated by
UNION CARBIDE CORPORATION
for the
ENERGY RESEARCH AND DEVELOPMENT ADMINISTRATION

CONTENTS

SUBSTRUCTURES DEVELOPED DURING CREEP AND CYCLIC TESTS OF TYPE 304 STAINLESS STEEL (HEAT 9T2796)*

R. W. Swindeman V. K. Sikka
R. K. Bhargava† J. Moteff†

ABSTRACT

Substructures developed in tested specimens of a reference heat of type 304 stainless steel (heat 9T2796) are examined. Data include dislocation densities, cell and subgrain sizes, and carbide precipitate sizes. Testing conditions range for temperatures from 482 to 649°C, for stresses from 28 to 241 MPa, and for times from 4 to 15,000 hr. As expected, it is observed that temperature, stress, and time have strong influences on substructure. The change in the dislocation density is too small to measure for conditions which produce less than 1% monotonic strain. No cells form, and the major alteration of substructure is the precipitation of $M_{23}C_6$ carbides on grain boundaries, on twin boundaries, and on some dislocations. At stresses ranging from 69 to 172 MPa and at temperatures ranging from 482 to 593°C, the dislocation density increases with increasing stress and is generally higher than expected from studies made at higher temperatures. Dislocations are arranged in fine networks stabilized by carbides. At stresses above 172 MPa and temperatures to 649°C, the dislocation density is too great to measure. Cells develop which are finer in size than cells developed at similar stresses but at higher temperatures. Dislocation densities and cell sizes for cyclic specimens are comparable to data for creep-tested specimens. On the basis of the observed substructures, recommendations are made regarding further studies which would assist in the development of constitutive equations for high-temperature inelastic analysis of reactor components.

INTRODUCTION

Currently recommended constitutive relations for use in the inelastic analysis of liquid-metal fast breeder reactor (LMFBR) components[1,2] are based on the assumption that mechanical strain can be separated into three components: elastic, time-independent plastic, and time-dependent creep. Specific constitutive relations which provide rules for describing the yield, flow, and hardening behavior are formulated separately for plasticity and creep. Ad hoc rules, which are intended to compensate for creep-plasticity interactions, are also provided. The equations are based primarily on concepts involving principles of continuum mechanics, thermodynamics, and rheology, although results from exploratory mechanical-property studies are also considered.[3] Although these constitutive equations have been accepted and are in use,[4] the Structural Design Methods (SDM) program[5] at the Oak Ridge National Laboratory (ORNL) is organized on the premise that the inelastic design methods should be upgraded periodically through an

*Work performed under ERDA/RDD 189a No. 0H048, High-Temperature Structure Design

†University of Cincinnati

1. C. E. Pugh et al., *Currently Recommended Constitutive Equations for Inelastic Design Analysis of FFTF Components*, ORNL-TM-3602 Oak Ridge National Laboratory (September 1972).

2. C. E. Pugh et al., *Background Information for Interim Methods of Inelastic Analysis for High-Temperature Reactor Components of 2¼ Cr 1 Mo Steel*, ORNL/TM-5226, Oak Ridge National Laboratory (1976).

3. J. M. Corum et al., *Pressure Vessels and Piping: Verification and Qualification of Inelastic Analysis Computer Programs*, pp. 13–25; 47–58; 79–109, ASME Publication G-00088, American Society of Mechanical Engineers, New York (June 1975).

4. U.S. Atomic Energy Commission, RDT Standard F9-5T, *Guidelines and Procedures for Design of Nuclear System Components at Elevated Temperatures*, Oak Ridge National Laboratory (March 1974).

5. W. L. Greenstreet, "ORNL High Temperature Structural Design Methods Development Program," *Trans. Am. Nucl. Soc.* 1(2): 400 (November 1973).

iterative process which requires a close interaction between material studies, constitutive equation development, computational methods development, and structural tests. The development of improved constitutive equations, for example, clearly requires an improved knowledge of material behavior.

Recently, Robinson and coworkers[6] have initiated work to develop improved constitutive equations for use in the LMFBR program. Under consideration are approaches proposed by Hart,[7] Onat,[8] Rice,[9] Lagneborg,[10] and Miller.[11] These last three investigators consider the fact that polycrystalline alloys deform principally by the movement of line defects (dislocations). However, in a commercial alloy, such as type 304 stainless steel at an elevated temperature, strong interactions occur between dislocations and point defects, such as interstitials and substitutional atoms. These interactions impede dislocation glide and climb. Also, as shown by Crossman and Ashby[12] and Mohamed and Langdon,[13] one can also expect that at low creep-strain rates, significant deformation can result from grain boundary sliding and diffusion creep, which do not necessary involve dislocation motion in the matrix. Finally, it is known that the presence of precipitates, such as $M_{23}C_6$, has a profound influence on the dislocation substructure[14,15] and hence, on mechanical behavior. These metallurgical complications have not been considered in the development of many of the deformation models advanced for predicting inelastic behavior of structural materials under arbitrary thermal and mechanical loadings. It would seem desirable, therefore, to characterize dislocation structure and to use such information as a guide in the selection of deformation models. The potential of this approach has been demonstrated recently by Lagneborg and coworkers.[16,17]

The work presented here represents an evaluation of dislocation substructures and carbide distributions in tensile, creep, and cyclic-tested specimens of type 304 stainless steel. The studies were supported by several ERDA programs, including a program at the University of Cincinnati on the Correlation of Strength and Microstructure (CSM) (ERDA contract no. AT-1011); and programs at Oak Ridge National Laboratory on the Generation and Correlation of Deformation and Failure Criteria for Structural Materials (DFCSM) (ERDA 189a 0H050), and the Development of Improved High-Temperature Inelastic Structural Design Method (SDM) for LMFBR Components (ERDA 189a Activity No. 0H048). In general, the specimens which were studied were not tested specifically to provide material for substructure investigations. Rather, the original intent was to produce mechanical properties data. Although the description of the thirty-six

---

6. D. N. Robinson, *A Candidate Creep-Recovery Model for 2¼ Cr–1 Mo Steel and Its Experimental Implementation*, ORNL-TM-5110, Oak Ridge National Laboratory (October 1975).

7. E. W. Hart, "A Phenomenological Theory for Plastic Deformation of Polycrystalline Metals," *Acta Metall.*, 18: 599–610 (1970).

8. E. T. Onat and F. Fardshisheh, *Representation of Creep of Metals*, ORNL-4783, Oak Ridge National Laboratory (August 1972).

9. J. R. Rice, "On the Structure of Stress-Strain Relations for Time-Dependent Plastic Deformation in Metals," *Trans. ASME, Ser. E. J. Appl. Mech.*, 37: 728–37 (1970).

10. R. Lagneborg, "A Modified Recovery-Creep Model and Its Evaluation," *Met. Sci. J.*, 6: 127–33 (1972).

11. A. K. Miller, "An Inelastic Constitutive Model for Monotonic, Cycle and Creep Deformation: Part I. Equations Development and Analytical Procedures; Part II. Application to Type 304 Stainless Steel," *Trans. ASME, J. Eng. Mater. Technol.*, 98: 97–113 (1976).

12. F. W. Crossman and M. F. Ashby, "The Non-uniform Flow of Polycrystals by Grain-Boundary Sliding Accommodated by Power-Law Creep," *Acta Metall.*, 23: 425–40 (1975).

13. F. A. Mohamed and T. G. Langdon, "Deformation Mechanism Maps Based on Grain Size," *Metall. Trans.*, 5: 2339–45 (1974).

14. J. T. Barnby, "Effect of Strain Aging on the High-Temperature Tensile Properties of an AISI 316 Austenitic Stainless Steel," *J. Iron Steel Inst. London*, 203: 392–65 (1965).

15. F. Garofalo, *Fundamentals of Creep and Creep Rupture in Metals*, MacMillan Co., New York, 1965.

16. R. Lagneborg, B-H. Forsén, and J. Wiberg, "A Recovery-Creep Model Based Upon Dislocation Distributions," pp. 1–7 in *Creep Strength in Steel and High Temperature Alloys*, The Metals Society, London, 1974.

17. A. Odén, E. Lind, and R. Lagneborg, "Dislocation Distributions During Creep and Recovery of a 20% Cr–35% Ni Steel at 700°C," pp. 60–66 in *Creep Strength in Steel and High Temperature Alloys*, The Metals Society, London, 1974.

transmission-electron micrographs reproduced in this report makes the reading somewhat tedious, the reader should take comfort in the fact that two hundred other available micrographs were not included.

MATERIAL AND EXPERIMENTAL TECHNIQUES

The material examined was taken from a 25-mm-thick plate of a well-characterized heat of type 304 stainless steel (heat 9T2796).[18] Uniaxial test bars having diameters near 6.35 mm were machined from the plate, reannealed for 0.5 hr at 1093°C, and tested in tensile, creep, and strain-cycling modes. All tensile tests were performed in air with techniques described elsewhere.[19] Although some tensile tests were discontinued at low strain levels, all the specimens examined here were tested to complete failure.

Creep tests were also performed in air using techniques described by Swindeman and Pugh.[20] Specimens which were examined included some on which tests were discontinued in different stages of creep, and some on which tests were continued to failure. When tests were discontinued, the load was maintained until the specimen was cool.

The experimental techniques used for cyclic testing have not been described previously. The specimen design and experimental setup are shown in Fig. 1. The cyclic specimen had a uniform length of 25 mm.

18. R. W. Swindeman, *Room-Temperature Characterization Data for Type 304 Stainless Steel (Heat 9T2796) Plate*, ORNL-TM-4396, Oak Ridge National Laboratory (February 1974).

19. R. W. Swindeman, *Low Strain Tensile Behavior of Type 304 Stainless Steel (Heat 9T2796)*, ORNL/TM-5245, Oak Ridge National Laboratory (February 1976).

20. R. W. Swindeman and C. E. Pugh, *Creep Studies on Type 304 Stainless Steel (Heat 8043813) Under Constant and Varying Loads*, ORNL/TM-4427, Oak Ridge National Laboratory (June 1974).

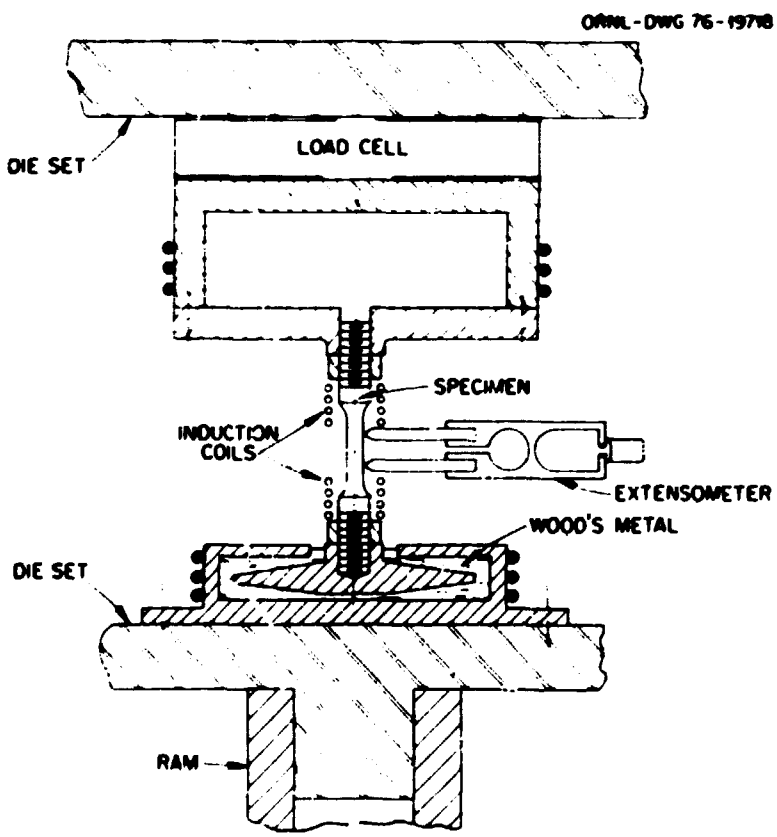

Fig. 1. Schematic drawing of setup for strain cycling.

about 10 mm of which was actually used for control of temperature and cyclic-strain range. The experimental setup was similar in many respects to the one used by Jaske et al.[21] Cyclic specimens were not tested to failure, but rather to cyclic lives which approached the values necessary to establish saturation conditions. Each test was terminated by unloading the specimen when it was halfway through the tensile portion of the hysteresis loop and then cooling the specimen to room temperature.

Specimens for transmission-electron microscopy (TEM) were prepared by cutting transverse sections from locations near the center of discontinued specimens or slightly away from the rupture surface of failed specimens. The diameters of slices were measured and used to determine the true stresses. The foils for TEM were prepared by mechanically thinning to foil thicknesses near 1 mm and by final electropolishing using a twin-jet polisher and an electrolyte of 90% acetic acid and 10% perchloric acid.[22] Several foils were examined when possible, and several areas of each foil were examined. Typically, micrographs of four to six areas were available for quantitative measurements.

The data base from which specimens were selected for this study is summarized by the matrix shown in Fig. 2. Temperatures range from 427 to 816°C and stresses from 35 to 414 MPa. The filled circles represent creep specimens studied in this work, and the filled squares represent creep specimens studied earlier.[22-24] The filled triangles represent tensile-tested specimens studied earlier. The open symbols represent test

21. C. E. Jaske, H. Mindlin, and J. S. Perrin, "Cyclic Stress-Strain Behavior of Two Alloys at High Temperature," pp. 13-27 in *Cyclic Stress-Strain Behavior – Analysis, Experimentation, and Failure Prediction*, Spec. Tech. Pub. 519, American Society for Testing and Materials, 1973.

22. Personal communication, R. K. Bhargava, University of Cincinnati, to R. W. Swindeman, Oak Ridge National Laboratory, 1975.

23. V. K. Sikka, C. R. Brinkman, and H. E. McCoy, "Effect of Thermal Aging on Tensile and Creep Properties of Types 304 and 316 Stainless Steel," pp. 316-50 in *Proc. 1974 Symp. Struct. Mater. Elevated-Temperature Nucl. Power Generation Service*, ed., A. O. Schaeffer, MPC-1, 1975.

24. R. Bhargava, R. W. Swindeman, and J. Moteff, "Correlation of the Microstructure with the Creep and Tensile Properties AISI 304 Stainless Steel," pp. 31-54 in *Symp. Struct. Mater. Elevated-Temperature Nucl. Power Generation Service*, ed., A. O. Schaeffer, MPC-1, 1975.

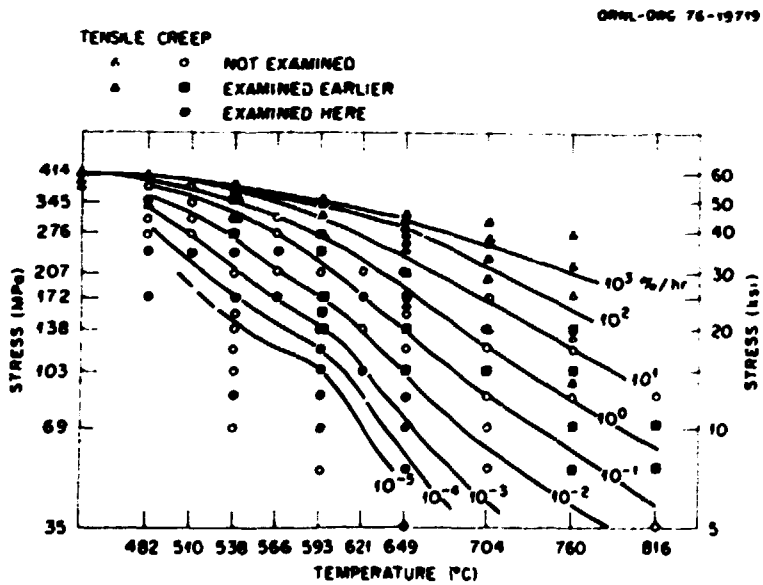

Fig. 2. Comparison of testing conditions for specimen examined in transmission-electron microscopy with the data base available for type 304 stainless steel (heat 9T2796).

specimens which were not examined. Superimposed on the matrix are curves which represent the creep strength vs temperature for secondary creep rates ranging from 10^{-5} to 10^{3} percent per hr. Figure 2 shows that specimens were selected for the examination of temperature effects at constant stress (for example, at 241, 172, and 103 MPa); stress effects at constant temperature (for example, at 538, 593, and 649°C); and stress-temperature effects at constant creep rate (for example, at 10^{-2}, 10^{-3}, and 10^{-4} percent per hr). The specimens included in this work (filled circles in Fig. 2) generally involved examination at lower temperatures than those in earlier studies.

RESULTS

Data generated at the University of Cincinnati under the support of the SDM program are summarized in Table 1. Included are data relating to the average cell or subgrain size (λ), the average dislocation density (ρ), and the size of the grain boundary and of the matrix carbides. In expanding the information contained in Table 1, we make use of data for the same material generated in the other programs described in the introduction. The information is organized on the basis of isothermal data, starting at the lowest temperature, 482°C (900°F), and moving upward. At each temperature we start with the lowest stress, considering at each stress level the shortest time first, then the longer times. Thus, we are examining the influence of increasing temperatures, increasing stresses (or plastic strains), and increasing times (or creep strains).

The initial microstructure is shown in Fig. 3. This consists of a low density of dislocations (approximately 10^{9} cm^{-2}) more or less randomly distributed throughout the grains. The grain size is approximately 180 μm, and the grain boundaries are free of precipitates.[18] There is some evidence of dislocations piled against or eminating from the boundaries in a few cases. Most dislocations are fairly straight, and there are few tangles, loops, or dipoles.

The first data listed in Table 1 are from a specimen (RP 125) tested at 172 MPa for 1580 hr. The test was discontinued after the specimen experienced about 5% loading strain and 0.03% creep strain. A typical TEM is shown in Fig. 4, and as can be seen, the dislocations (7.55×10^{9} cm^{-2}) lie primarily on slip traces (111 planes). There are quite a few curved dislocations and some tangles, loops, and dipoles. No clear evidence of dislocation cells or subgrains exists. Possibly this structure has been produced by planar slip during plastic loading, followed by cross slip and glide of dislocations out of the slip plane during the period of creep. There is no evidence of precipitation in either the grain boundaries or the matrix at the magnifications which were employed (20,000 ×). This is consistent with the finding of Sikka et al.[23] on material aged at 482°C (900°F).

The second data listed in Table 1 comes from a specimen (RP 267) tested at 482°C and 241 MPa. This specimen experienced about 8% loading strain and about 0.06% creep strain. The specimen did not rupture. The substructure shown in Fig. 5 differs markedly from the substructure developed at lower stress (Fig. 4) and consists of a high density of dislocations which are tangled in a configuration of poorly defined cell walls. The average cell dimension is estimated at 0.72 μm. The cellular structure seen in Fig. 5 is a result of the large plastic loading strain and is more a manifestation of dislocation glide and dynamic recovery processes which involve cross slip than a manifestation of dislocation climb and thermal recovery. Although no grain boundary precipitates are observed, a few localized needles which could be $M_{23}C_6$ carbides are present. The major dimension of the needles is near 0.5 μm.

Data for one specimen (RP 324), tested at 510°C (950°F) and 241 MPa, are reported in Table 1. This specimen experienced about 10.4% loading strain and failed in 3511 hr. The substructure which developed in this specimen (Fig. 6) consists of poorly defined cells, having an intercept dimension near 0.92 μm, and being aligned more or less along cystallographic planes. The dislocation density is not reported but appears

Table 1. Data produced by transmission-electron microscopy examination of creep tested specimens of type 304 stainless steel (NT 9T2796)

Specimen number	Temperature (°C)	Engineering stress (MPa)	Modulus-compensated true stress[a] $(\sigma/G) \times 10^3$	Loading strain[b] (%)	Creep strain (%)	Time[c] (hr)	Average cell or subgrain size, λ (μm)	Dislocation density,[d] ρ (10^{14} m^{-2})	Matrix carbide size (μm)	Grain boundary carbide size (μm)
RP 135	482	172	2.77	5.0	0.03	1580 (P)	NO[e]	7.55 ± 2.0	NO	NO
RP 267	482	241	3.92	8.0	0.06	1001 (P)	0.72 ± 0.10	NM[e]	ST[e]	NO
RP 324	510	241	4.18	10.4	2.50	3511 (R)	0.92 ± 0.09	NM	ST	0.1
RP 78 (shoulder)	538	41	0.68	nil	nil	11540 (P)	NO	NM	0.04 +0.03 −0.01	< 0.04
RP 264	538	86	1.42	nil	0.06	5000 (P)	NO	1.09 ± 0.35	ST	<0.2 +0.12 −0.05
RP 78	538	172	3.03	5.5	1.9	11540 (T)	NO	10.5 ± 2.6	0.04 +0.02 −0.01	<0.2 +0.07 −0.08
RP 251	538	241	4.64	11.6	6.4	350 (R)	0.76 ± 0.05	NM	NO	<0.12 +0.06 −0.02
RP 320	566	172	3.22	5.2	7.8	2054 (R)	NO	8.1 ± 2.0	0.035 ± 0.015[f]	0.2 +0.02 −0.08
RP 270	566	241	4.62	10.5	9.5	114 (R)	0.83 ± 0.08	NM	NO	0.08
RP 213	593	28		nil	nil	15500 (P)	NO	NM	0.09	0.4
RP 28	593	69	1.18	0.16	0.22	5031 (P)	NO	NM	0.08 +0.06 −0.03	0.3
RP 215	593	69	1.18	0.18	0.29	5008 (P)	NO	NM	0.08 +0.07 −0.05	0.2 +0.08 −0.01
RP 216	593	86	1.47	0.88	0.48	5006 (P)	NO	3.4 ± 1.0	0.17 +0.03 −0.02	0.3 < 0.1
RP 79	593	103	1.8	1.6	0.95	5014 (P)	NO	4.75 ± 1.5	0.065 +0.015 −0.005	NM
RP 133	593	121	2.12	2.4	0.75	1027 (P)	NO	4.88 ± 1.2	0.035 +0.025 −0.005	NM
RP 40	593	121	2.17	2.8	2.2	5131 (S)	NO	4.66 ± 1.3	0.07 +0.05 −0.01	0.2
RP 213	593	121	2.18	2.3		15500 (R)	NO	5.83 ± 1.7	0.09 +0.03 −0.025	0.4
RP 58	593	138	2.35	2.8	5.8	5060 (T)	NO	4.82 ± 1.21	0.05 +0.03 −0.01	0.28 +0.02 −0.03
RP 54	593	172	3.24	5.5	5.5	402 (T)	NO	7.4 ± 2.0	0.04 +0.03 −0.01	NM
RP 43	593	172	3.42	4.5	11.5	619 (R)	0.87 ± 0.09	6.0 ± 1.4	0.04 ± 0.02	0.25
RP 166	593	207	4.07	7.3	13.7	98.5 (R)	NO	10.1 ± 2.5	NO	0.12 ± 0.03
RP 266	621	103	2.07	1.31	16.7	4595 (R)	2.21 ± 0.16	2.64 ± 0.66	0.10 +0.05 −0.02	NM
RP 263	621	172	3.49	5.0	17	119 (R)	NO	12.5 ± 3.1	0.04 ± 0.02	NM
RP 158	649	35	0.61	nil	0.238	10000 (P)	NO	0.89 ± 0.22	0.20 +0.1 −0.07	0.5
RP 126	649	51	0.92	nil	0.66	10000 (P)	NO	0.83 ± 0.20	0.23 +0.12 −0.08	0.5
RP 144	649	69	1.22	0.15	5.6	8232 (T)	2.57 ± 0.3	NM	0.14 +0.02 −0.03	0.5
RP 247	649	86	1.69	0.88	12.1	2500 (T)	2.45 ± 0.4	3.33 ± 0.8	0.13 +0.02 −0.01	0.47
RP 87	649	86	1.83	0.82	21.2	3960 (R)	1.99 ± 0.3	2.68 ± 0.67	0.135 +0.015 −0.035	0.5

[a] Axial stress/Shear modulus

[b] Inelastic strain only

[c] Letters in parentheses indicate creep stage. P = primary, S = secondary, T = tertiary, R = rupture

[d] Refers to dislocations not associated with cell walls or subgrain boundaries

[e] NO = not observed, NM = not measured

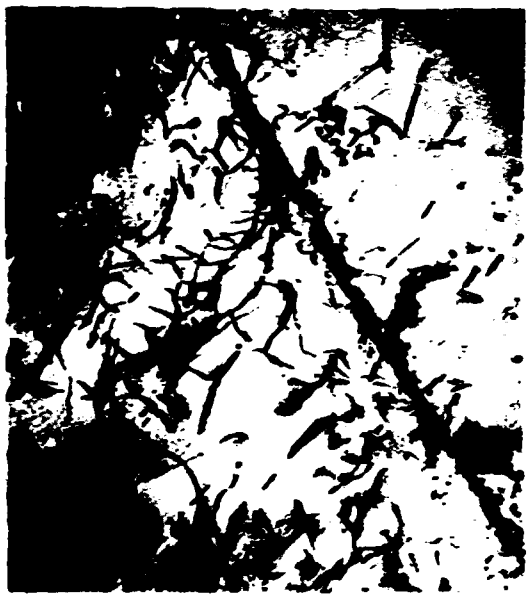

Fig. 3. Reannealed condition, ρ near 10^{9} cm^{-2}, (25,000×)

Fig. 4. RP 125 tested at 482 °C at 172 MPa for 1580 hr, 5.03% strain. ρ near 7.5×10^{9} cm^{-2}, (20,000×)

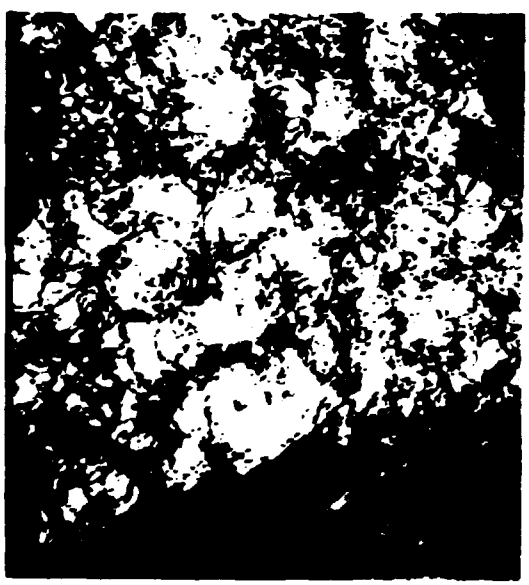

Fig. 5. RP 267 tested at 482 °C at 241 MPa for 1001 hr, experiencing 8.06% strain. λ near 0.72 μm (20,000×)

Fig. 6. RP 324 tested at 510 °C at 241 MPa for 3511 hr, experiencing 12.9% strain. λ near 0.92 μm. (15,000×)

qualitatively to be similar to the density observed in the high-stress specimen (RP 267) tested at 482°C and shown in Fig. 5. As before, the substructure is developed primarily from the large plastic loading strain which produced dislocation glide, cross slip, and associated dynamic recovery. Precipitation of carbides occurs on the grain boundaries at this temperature, however, and a typical size is near 0.1 μm. There is also some evidence of matrix carbides. These are few, localized, and near 0.1 μm in size.

At 538°C (1000°F), the substructures developed at eight stress levels have been examined. Two stress levels (specimens RP 14 and RP 201) were produced by tensile testing. These and several creep specimens have been examined under the sponsorship of a different program (CSM) and data are not included in Table 1. The substructure for the lowest stress (near 41 MPa) listed in Table 1 was produced in the shoulder region of a specimen (RP 78) tested at 172 MPa for 11,540 hr. This substructure is shown in Fig. 7 and exhibits the same dislocation density as the untested specimen. The dislocations are straight, exhibit attractive junctions, and are decorated by precipitates approximately 0.03 to 0.06 μm in size. The cell size is the same as the grain size. Precipitates also lie on the grain boundaries and appear to be of the same size as matrix precipitates. These precipitates are associated with boundary dislocations.

The next stress level examined at 538°C (1000°F) is 86 MPa (specimen RP 264). The specimen experienced no plastic loading strain, but accumulated about 0.06 creep strain before the test was discontinued at 5000 hr. There is no evidence in Fig. 8 of subgrains, and the dislocation density (1.09×10^9 cm^{-2}) is close to the starting value. The dislocations are arranged in networks having both attractive and repulsive junctions.[17,25] Curved dislocation segments appear to be free of precipitates. There is some evidence that fine precipitates are present on some matrix dislocations, as is the case for the shoulder region of specimen RP 78, described above. These precipitates are about 0.02 μm in size.

The section of specimen RP 78 which was stressed to 172 MPa experienced about 5.5% plastic loading strain and 1.9% creep strain before the test was discontinued in the tertiary creep stage. The dislocation substructure shown in Fig. 9 can be best described as a dense dispersion of tangles and networks. There are numerous repulsive junctions, loops, and dipoles. The substructure appears to be stabilized by carbide precipitates, shown in Fig. 10. All evidence of the planar slip produced during loading has been destroyed. Some relatively clear areas among the tangles might be considered as intercell regions, however. The dislocation density is about one order of magnitude above the initial value, and the substructure does not suggest that thermal recovery processes are very active. It is clear that the carbide dispersion is fine enough to play a role in determining the time-dependent behavior.

The final data in Table 1 for 538°C describe the substructure developed in a specimen stressed to 241 MPa. The plastic loading strain is 11.8%, and the creep strain about 6.4%. The specimen failed in 350 hr. The substructure, shown in Fig. 11, exhibits characteristics similar to the substructure developed at 482 and 510°C at the same nominal stress level. The average cell size is near 0.76 μm, and perhaps cells walls are more clearly defined than at lower temperatures. The dislocation density is too high to conveniently measure. This substructure is consistent with the dislocation glide, cross slip, and dynamic-recovery deformation mechanism. Carbides are present on the boundaries and are approximately 0.12 μm in size.

Other specimens examined by Bhargava and coworkers[26,27] include three creep specimens (RP 8 at 276 MPa, RP 9 tested at 241 MPa, and RP 26 tested at 138 MPa) and two tensile specimens (RP 14, with an ultimate strength near 385 MPa; and RP 201, with an ultimate strength near 362 MPa). Specimens RP 201, RP 14, and RP 8, which were tested at high stresses, exhibit cell-type substructures, while the specimens at the two lower stresses exhibit what Bhargava et al.[26] call "mixed" substructures. This is a configuration in which cell walls are more sharply defined than at low temperatures and take on more of a subgrain character.

---

25. R. Lagneborg, "Dislocation Mechanisms in Creep," *Int. Metall. Rev.*, 11: 130–46 (1972).

26. R. K. Bhargava, J. Moteff, and R. W. Swindeman, "The Dislocation Substructure, Carbides, and the Deformation Map for AISI 304 Stainless Steel," *Metall. Trans.*, 7A: 879–84 (1976).

27. T. Kenfield, University of Cincinnati, to R. W. Swindeman, Oak Ridge National Laboratory, 1975.

Fig. 7. RP 78s tested at 538°C at 41 MPa for 11,540 hr. No strain. (15,000×)

Fig. 8. RP 264 tested at 538°C at 86 MPa for 5000 hr. 0.0% strain. ρ near 1×10^{9} cm^{-2}. (20,000×)

Fig. 9. RP 78 tested at 538°C at 172 MPa for 11540 hr. 7.4% strain. ρ near 10.5×10^{9} cm^{-2}. (15,000×)

Fig. 10. RP 78 tested at 538°C at 172 MPa for 11540 hr. 7.4% strain. $M_{23}C_6$ precipitates. (20,000×)

Fig. 11. RP 251 tested at 538°C at 241 MPa for 350 hr. 18% strain. λ near 0.76 μm. (15,000×)

Fig. 12. RP 320 tested at 566°C at 172 MPa for 2054 hr. 13% strain. ρ near 8.1×10^{9} cm^{-2}. (20,000×)

Fig. 13. RP 270 tested at 566°C at 241 MPa for 114 hr. 20% strain. λ near 0.83 μm. (15,000×)

Fig. 14. RP 215 tested at 593°C at 69 MPa for 5008 hr with 0.47% strain. (20,000×)

Two specimens tested at 566° C (1050°F) have been examined, and the data have been reported in Table 1. The low-stress test specimen (RP 320) at 172 MPa experienced 5.2% plastic loading strain and 7.8% creep strain before rupturing after 2054 hr. The substructure, shown in Fig. 12, consists of curved dislocation tangles which are stabilized by the presence of a dispersion of carbides. There are some repulsive junctions and loops, but all evidence of the planar slip associated with the plastic loading strain is absent. The substructure is similar to that developed at 538°C (RP 78). Large carbides are also present on the grain boundaries. The high-stress test specimen (RP 270) at 241 MPa experienced 10.5% loading strain and 9.5% creep strain. Cells are present as shown in Fig. 13, but a rather high dislocation density exists within the cells. The structure is again indicative of glide processes, and there is no evidence that thermal recovery plays a significant role in the deformation process.

A substantial amount of data are available at 593°C (1100°F). Substructures developed after aging for times up to 10,000 hr have been examined by Sikka et al.[23,28] who have determined precipitate sizes on grain boundaries, on twin boundaries, and within the matrix of this material. With respect to the influence of stress, data determined from studies on eleven specimens are provided in Table 1. Results from a study on an additional six specimens, including two tensile tests, are reported by Bhargava et al.[26] The lowest stress reported in Table 1 is near 28 MPa, which corresponds to the stress in the shoulder region of specimen RP 213 which ruptured in 15,500 hr. The microstructure of this specimen, not provided here, is similar to the shoulder region of RP 78. Results from two specimens tested at 69 MPa for 5000 hr are summarized in Table 1. Both specimens RP 28 and RP 215 experienced small plastic loading strains, 0.16 and 0.18% respectively, and accumulated creep strain less than 0.3%. Substructures of the specimens, which are very similar, are shown in Fig. 14. The dislocation densities are near the starting value, and no subgrains are present. Dislocation networks with attractive junctions are decorated with precipitates of a size near 0.08 μm. Within these networks curved dislocations without precipitates exist. The deformation mechanism producing this structure could be the thermally activated breaking of nodal points on the networks and the subsequent glide and recombination of dislocations within the stabilized networks.[16] Clearly, the carbide precipitate stabilizes the dislocation substructure, but it is questionable whether the precipitates contribute directly to creep hardening. An increase in hardness after long-time aging was observed by Sikka et al.,[23] however, implying that the precipitate is hardening with respect to plastic flow.

Very similar substructures are developed after creep testing at stress levels ranging from 86 to 138 MPa. The plastic loading strains range from 0.88% for specimen RP 216 at 86 MPa, to 2.8% for specimen RP 58 at 138 MPa. Creep strains, reported in Table 1, range from 0.48 to 5.8% for specimens RP 216 to RP 58, respectively. Typical substructures developed in the six specimens are shown in Figs. 15 through 20. Neither cells nor subgrains have developed in any of the specimens, but the dislocation density in the specimens discontinued after approximately 5000 hr increases by about 40% when there is a 60% increase in stress. Three specimens tested at 121 MPa for different times (creep strain) exhibit nearly the same dislocation density at 1027 and 5131 hr, but show a higher value at 15,500 hr. Substructures consist of short and curved dislocation segments joined in a network of small tangles with many repulsive junctions. A few loops and dipoles are also present. The precipitates often lie on what were once slip traces or on long straight dislocations. Matrix-carbide sizes are relatively independent of stress, but range with time from 0.035 μm at 1027 hr to 0.09 μm at 15,500 hr. Typical substructures for specimens RP 43 and RP 166 are shown in Figs. 21 and 22. Figure 21 represents the substructure developed after 619 hr at 172 MPa, and Fig. 22 shows substructure development after 98.5 hr at 207 MPa. The dislocation densities are greater than those observed at lower stresses, and the substructures are quite variable. Some foils exhibit intense tangles, perhaps stabilized by the precipitation of fine carbides, while in other areas discernible cells are present. Often the precipitates are aligned on what were once slip bands. Because of the shorter times involved, the matrix precipitates tend to be smaller at these high stresses. Substructural features for high-stress tests at

28. V. K. Sikka and C. R. Brinkman, *Uniaxial Tensile Properties of Austenitic Stainless Steels Following Prior Creep Deformation — An Interim Report*, ORNL/TM-5193, Oak Ridge National Laboratory (April 1976).

Fig. 15. RP 216 tested at 593°C at 86 MPa for 5006 hr with 1.36% strain. ρ near 3.4 × 10^9 cm $^{-2}$. (20,000×)

Fig. 16. RP 79 tested at 593°C at 103 MPa for 5014 hr with 2.55% strain. ρ near 4.75 × 10^9 cm $^{-2}$. (15,000×)

Fig. 17. RP 133 tested at 593°C at 121 MPa for 1027 hr with 3.15% strain. ρ near 4.88 × 10^9 cm $^{-2}$. (15,000×)

Fig. 18. RP 40 tested at 593°C at 121 MPa for 5131 hr with 5.0% strain. ρ near 4.66 × 10^9 cm $^{-2}$. (20,000×)

Fig. 19. RP 213 tested at 593 C at 121 MPa for 15,500 hr with 5.6% strain. ρ near 5.83×10^{9} cm^{-2}. (15,000×)

Fig. 20. RP 58 tested at 593 C at 138 MPa for 5060 hr with 8.6% strain. ρ near 4.82×10^{9} cm^{-2}. (20,000×)

Fig. 21. RP 43 tested at 593°C at 172 MPa for 619 hr with 16% strain. ρ near 6.0×10^{9} cm^{-2}. (30,000×)

Fig. 22. RP 166 tested at 593°C at 241 MPa for 98.5 hr with 21% strain. ρ near 10.1×10^{9} cm^{-2}. (40,000×)

593°C are also summarized by Bhargava et al.[26] Dislocations tend to exhibit "mixed" or cellular configurations. The tensile tests exhibit cellular substructures with few, if any, matrix carbides.

Two specimens tested at 621°C (1150°F) have been examined with the data summarized in Table 1. The low-stress test specimen (RP 266) ruptured in 4595 hr at 103 MPa. The plastic loading strain is 1.3%, and the creep strain is 16.7%. The substructure (Fig. 23) differs markedly from substructures produced by the same stress at lower temperatures. (See Fig. 15, for example). At 621°C (1150°F), well-defined subgrains develop. Within the subgrains, dislocation networks exist which often exhibit attractive junctions. This type of substructure is typical of high-temperature deformation where thermal-recovery processes, especially dislocation climb, are very active. The dislocation density of 2.64×10^9 cm^{-2} within the grains is low. This substructure is somewhat surprising and may indicate that the temperature controller malfunctioned and produced overheating. This had to happen very quickly, however, because independent monitoring of temperatures occurs on a daily basis, and no temperature excursion was observed. The substructure exhibited by the high-stress test (RP 263) is similar to that observed for the same stress (172 MPa) at lower temperatures. This consists of areas where intense tangling develops amid a dispersion of matrix carbides. The typical substructure is represented in Fig. 24.

The substructures developed in specimens tested at 649°C (1200°F) are consistent with data widely available in the literature for austenitic stainless steels.[29-32] Our study included five specimens tested in the stress range of 35 to 86 MPa for times up to 10,000 hr. Supplementary data have been reported by Moteff and coworkers[33,26] for stresses in the range of 103 to 321 MPa, including four tensile tests at different strain rates.

With respect to aging alone, Sikka et al.[28] have observed the precipitation of carbides for times up to 10,000 hr and have reported an increase in the hardness, yield strength, and creep rate as a consequence of this precipitation. The substructure is virtually the same under low-stress creep conditions as for aging without stress; a typical substructure (RP 158) for a test at 35 MPa and 10,000 hr is shown in Fig. 25. The specimen experienced no plastic loading strain and only 0.238% creep strain. The dislocation density for this specimen and for one tested for 10,000 hr at 51 MPa is essentially the same as for an unstressed specimen. The precipitates are very large, near 0.2 μm, and are not distributed along dislocations. The precipitates usually have a curved dislocation associated with them. Both attractive and repulsive junctions are observed in the dislocation network, and in a few instances extended nodes are present. The substructure in the specimen (RP 126) stressed at 51 MPa for 10,000 hr is shown in Fig. 26. It is similar in almost all respects to the substructure developed at 35 MPA (RP 158). At 69 MPa, however, the substructure assumes a new character, as observed in specimen RP 144 which accumulated about 5% creep strain in reaching the tertiary creep stage around 8000 hr. The substructure in Fig. 27 consists of subgrains, with precipitates sometimes decorating the walls. The dislocation network within the subgrains has segments which are sometimes straight and sometimes curved; a fairly high density of attractive junctions is present. The large matrix carbides usually have dislocations associated with them. The substructure suggests that the deformation is dominated by thermal-recovery processes, such as dislocation climb.

Two specimens, RP 87 and RP 247, were tested at 86 MPa. Both specimens experienced about the same plastic loading strain, but the creep strain for specimen RP 247, which was discontinued slightly into the tertiary creep stage, is about half that of RP 87, which was tested to failure. The substructures for the specimens are similar and consist of well defined subgrains containing dislocation networks. The substructure shown in Fig. 28 is typical. The network segments vary in character and are sometimes curved

29. F. Garofalo et al., "Strain-Time, Rate-Stress, and Rate-Temperature Relations during Large Deformations in Creep," pp. 1-31 in *Joint Int. Conf. Creep*, Inst. Mech. Eng., London, 1963.

30. L. J. Cuddy, "Internal Stresses and Structures Developed During Creep," *Metall. Trans.*, 1: 395-401 (1970).

31. S. N. Monteiro and H. J. Kestenbach, "Influence of Grain Orientation on the Dislocation Substructure in Austenitic Stainless Steel," *Metall. Trans.*, 6A: 938-40 (1975).

32. T. L. da Silveira and S. N. Monteiro, "Strengthened Creep Substructures in 316 Stainless Steel," pp. 334-38 in *2nd Int. Conf. Mech. Behavior of Metals*, American Society of Metals, 1976.

Fig. 23. RP 266 tested at 621°C at 103 MPa for 4595 hr with 18% strain. ρ near 2.64 × 10^{9} cm^{-2}. λ near 2.21 μm (15,000×)

Fig. 24. RP 263 tested at 621°C at 172 MPa for 119 hr with 22% strain. ρ near 12.5 × 10^{9} cm^{-2}. (20,000×)

Fig. 25. RP 158 tested at 649°C at 35 MPa for 10,000 hr with 0.2.8% creep strain. ρ near 0.89 × 10^{9} cm^{-2}. (15,000×)

Fig. 26. RP 126 tested at 649°C at 51 MPa for 10,000 hr with 0.66% creep strain. ρ near 0.83 × 10^{9} cm^{-2}. (15,000×)

Fig. 27. RP 144 tested at 649°C at 69 MPa for 8232 hr with 5.75% strain. λ near 2.57 μm. (15,000×)

Fig. 28. RP 87 tested at 649°C at 86 MPa for 3960 hr with 22% creep strain. ρ near 2.68 × 10⁹ cm⁻² λ near 1.99 μm. (20,000×)

Fig. 29. FRP 107 tested at 427°C at 0.37% Δe for 1000 cycles at 148 MPa. ρ near 7.66 × 10⁹ cm⁻². λ near 1.46 μm (10,000×)

Fig. 30. FRP 107 tested at 427°C at 0.37% Δe for 1000 cycles at 148 MPa.(30,000×)

and sometimes straight as when tested at 69 MPa. Both attractive and repulsive junctions are present, and extended dislocation nodes are occasionally observed. Large blocky matrix carbides are present and are usually surrounded by dislocation tangles. Substructures developed in creep and tensile tests at stresses of 103 and 138 MPa consist of subgrains, with walls sometimes decorated by precipitates. Dislocations within the subgrains are often straight with attractive junctions. Matrix precipitates form rows, suggesting that they developed on slip traces produced during loading. The substructures indicate that the creep deformation at 649°C (1200°F) is controlled by thermal-recovery processes, such as dislocation climb. As stresses are increased, however, subgrains give way to cells, and the matrix precipitates become smaller as testing times become shorter. Additional data pertaining to the development of substructures under creep and tensile conditions are available elsewhere[24,25] for temperatures of 704, 760, and 816°C. Depending on the stress, either subgrains or cells are formed and precipitates, when they develop, are characteristically very large.

Just as microstructural data are needed for the early stages of creep at temperatures and stresses of concern to the LMFBR program, so also are microstructural data needed which pertain to the early stages of cyclic hardening at similar temperatures. The studies here represent a preliminary scoping. Data from six cyclic specimens are summarized in Table 2, which provides cell or subgrain intercept values, dislocation

Table 2. Data produced by transmission-electron microscopy examination of strain cycled specimens of type 304 stainless steel (heat 9T2796)

Specimen number	Temperature (°C)	Cyclic strain range[a] (%)	Engineering stress amplitude[b] (MPa)	Modulus-compensated true stress[c] (10^{-3})	Cycles	Cell size λ (μm)	Dislocation density ρ (10^9/cm^2)	Grain boundary carbide (μm)
FRP 107	427	0.37	148	2.55	1000	1.46 ± 0.32	7.66 ± 1.76	NO[d]
FRP 106	482	0.37	154	2.35	10000[e]	1.23 ± 0.21	5.39 ± 1.26	NO
FRP 115	538	0.37	172	2.84	<2000	1.13 ± 0.30		NM[d]
FRP 110	649	0.375	132	2.34	1000	2.24 ± 0.32	4.34 ± 1.08	NM
FRP 109	649	0.62	150	2.65	100	1.68 ± 0.15	7.08 ± 1.80	NO
FRP 111	649	0.89	161	2.85	100	1.63 ± 0.10	6.55 ± 1.62	NO

[a]Strain rate near 8.3×10^{-5}/sec.

[b]Stress value close to the saturation condition.

[c]Axial stress amplitude/shear modulus.

[d]NO = not observed, NM = observed but not measured.

[e]Approximately 1000 cycles at 8.3×10^{-5} and 9000 cycles at 4.3×10^{-3}/sec.

densities and carbide-precipitation behavior. Four specimens (FRP 107, FRP 106, FRP 115, and FRP 110) were cycled at a total strain range near 0.37% at 427, 482, 538, and 649°C, respectively. Two specimens, FRP 109 and FRP 111, were cycled at higher strain levels at 649°C. Test times at the 0.37% strain range were similar, although one test specimen (FRP 106) was carried to 10^4 cycles by increasing the test frequency after 10^3 cycles. Transmission-electron micrographs for the specimen tested at 427°C are shown in Figs. 29 and 30. The substructure consists of tangles of dislocations occurring at the intersection of slip traces (Fig. 29). The high-magnification micrograph (Fig. 30) reveals the presence of loops, dipoles, and multipoles. These features are typical of the early stages of cyclic hardening observed by Nahm et al.[33] Although a well-defined cell structure has not developed, there is sufficient delineation to permit an estimate of the cell-size limit (λ), which is near 1.46 μm. Misorientation occurs between the cells in some cases and a typical angle is near 0.1 degree. The dislocation density, ρ, is near 7.7×10^9 cm^{-2}, and no evidence of a precipitate exists in either the grain boundaries or in the matrix. The substructure developed

33. H. Nahm, J. Moteff, and D. R. Diercks, "Substructural Development During Low-Cycle Fatigue of AISI 304 Stainless Steel at 649°C," *Acta Metall.* 25: 107–16 (1977).

at 482°C (FRP 106) and shown in Fig. 31 is similar to that developed at 427°C. Although the cyclic-stress range is virtually the same, both the cell size and the dislocation density are smaller in the 482°C tested specimen. It is not clear whether this discrepancy reflects the differences in the temperature or the total accumulated plastic strain. Also, it is possible that more foils need to be examined.

Tests conducted at 538°C (FRP 115) show that the cyclic-stress range is substantially greater than at 427 and 482°C. The substructure shows regions where cell walls are well-defined, as illustrated in Fig. 32. Other areas are similar in substructure to the lower temperatures as illustrated in Fig. 33. Loops, dipoles, and multipoles are present. The cells are only slightly smaller than cells at 482°C, in spite of the higher cyclic stress, but the range of cell sizes at a single temperature is large relative to the differences in the averages at the various temperatures. The substructure is consistent with the observation of Moteff and coworkers[33-35] that the cells tend to develop near the grain boundaries first and then move inward. Figure 32 reveals the presence of grain boundary carbides about 0.1 μm in size.

The specimen (FRP 110) cycled at 649°C and at the 0.375% strain range exhibits a lower saturation stress range than at lower temperatures. On a modulus-compensated true-stress basis, however, the stress range is about the same as the range at temperatures of 427 and 482°C. The cell size is greater, and the dislocation density is lower in the specimen cycled at 649°C. Typical substructures are shown in Figs. 34 and 35. These reveal that the cellular structure is in a primitive stage of development in spite of the fact that the specimen was cycled well into the saturation-stress range. The substructure consists of bundles and tangles, with dipoles and multipoles. Loops are present, some of which are very small and could ever be matrix carbides. Occasionally extended nodes are encountered. The grain boundaries contain precipitates as would be expected from the test duration.

Specimens cycled at higher strain levels at 649°C exhibit some regions similar to those observed in the low strain tests. Typical regions of this type are illustrated in Fig. 36 for the specimen cycled at 0.62%

Fig. 31. FRP 106 tested at 482°C at 0.37% Δε for 10,000 cycles at 152 MPa. ρ near 5.39 × 10⁸ cm⁻². λ near 1.23 μm. (10,000×)

Fig. 32. FRP 115 tested at 538°C at 0.37% Δε for 2000 cycles at ±172 MPa. λ near 1.13 μm. (10,000×)

34. K. D. Challenger and J. Moteff, "Characterization of the Deformation Substructure of AISI 316 Stainless Steel After High Strain Fatigue at Elevated Temperatures," *Metall. Trans.*, 3: 1675–78 (1972).

35. K. D. Challenger and J. Moteff, "Correlation of Substructure with Elevated Temperature Low-Cycle Fatigue of *AISI 304 and 316 Stainless Steel*," *Fatigue at Elevated Temperatures*, STP 520, American Society for Testing Materials, Philadelphia, 69–78 (1973).

Fig. 33. FRP 115 tested at 538°C at 0.37% $\Delta\varepsilon$ for 2000 cycles at ±172 MPa. (7500×)

Fig. 34. FRP 110 tested at 649°C at 0.375% $\Delta\varepsilon$ for 1000 cycles at ±132 MPa. ρ near 4.34×10^{9} cm^{-2}, λ near 2.24 μm. (7500×)

Fig. 35. FRP 110 tested at 649°C at 0.375% $\Delta\varepsilon$ for 1000 cycles at ±132 MPa. (20,000×)

Fig. 36. FRP 109 tested at 649°C at 0.62% $\Delta\varepsilon$ for 100 cycles at ±150 MPa. ρ near 7.08×10^{9} cm^{-2}, λ near 1.68 μm. (15,000×)

Fig. 37. FRP 111 tested at 649°C at 0.89% $\Delta\varepsilon$ for 100 cycles at ±161 MPa. ρ near 6.55 × 10^{9} cm^{-2}, λ near 1.63 μm. (10,000×)

Fig. 38. FRP 109 tested at 649°C at 0.62% $\Delta\varepsilon$ for 100 cycles at ±150 MPa. (7500×)

Fig. 39. FRP 111 tested at 649°C at 0.89% $\Delta\varepsilon$ for 100 cycles at ±161 MPa. (7500×)

strain range, and in Fig. 37 for the specimen cycled at 0.89% strain range. Both figures reveal the presence of tangles, dipoles, and loops arranged in a configuration of primitive cells. The subcell sizes and dislocation densities are similar to those observed at lower temperatures and similar stress ranges. Some regions in the specimens cycled at 649°C exhibit well-defined cell walls such as those shown in Figs. 38 and 39 for 0.62 and 0.89% strain ranges, respectively. An interesting feature is that some cells contain curved dislocations which reach almost from one wall to another; these could be gliding dislocations which have broken free of one cell wall and are moving toward another. However, the substructure and deformation mechanisms

associated with cyclic deformation in this material have been studied by Nahm et al.[33] who suggest that the cyclic deformation is dominated by dislocation movement in the cell walls. Many more studies of behavior in the early hardening stages are necessary before any of several conceivable hardening models[36–39] for cyclic behavior can be identified.

DISCUSSION AND ANALYSIS

In describing the substructures developed by various combinations of temperature, stress, and strain rate, we have mentioned some possible deformation mechanisms which are consistent with the substructural observations. We have not been very specific, however, and do not feel that our knowledge has progressed to a stage where the operative deformation mechanisms can be confidently identified and used to develop constitutive equations. One of the problems is that the majority of the deformation mechanisms, such as those used by Ashby[40] to develop deformation maps, apply to "steady-state" conditions. This is an unlikely event in a structural component of an LMFBR, which undergoes numerous transients during its service life. These transients are what introduce the plastic strains and residual stresses which relax by creep. Ideally, the developer of constitutive equations should understand, mechanistically, the nature of plasticity and creep deformations and how they interact. An important question relative to the current constitutive relations is whether or not separation of creep and plasticity is really essential. If not, we must decide whether it is proper to separate the plasticity and creep simply for computational convenience. The substructure study presented here does not provide final answers to these problems, but when combined with the existing knowledge of mechanical behavior, it does represent a step in the right direction toward reaching a proper solution.

Consider the isochronous stress-strain behavior for reannealed type 304 stainless steel. Typical curves are shown in Fig. 40 at initial loading (zero) time and after 5000 hr. This material has a very low elastic limit (point A) and often exhibits an accommodation strain region (A to B). Reed-Hill[41] cites the work of Zankl,[42] who describes large grains favorably orientated for slip which undergo plastic yielding before general yielding. Dislocations on active slip planes within the "weak" grains impinge on grain boundaries and trigger accommodation slip in neighboring grains. Yield-surface studies employed to develop hardening rules for multiaxial stress states are generally restricted to small inelastic strains in this accommodation range, about 10×10^{-6} to 50×10^{-6} offset strain.[43] In relation to the creep strength, the stresses produced by these surface probes are very low. Reannealed austenitic steels also exhibit general yielding at stresses which are low in relation to the creep strength, approximately 70 MPa in the temperature range of 450 to 650°C (point B). This general yielding occurs by planar slip, and in small-diameter test bars deformation is often not homogeneous, but sweeps up and down the uniform test section in a series of

36. J. C. Grosskreutz, "The Mechanisms of Metal Fatigue (I)," *Phys. Stat. Sol.* 47: 11–30 (1971).

37. C. F. Feltner, "A Debris Mechanism of Cyclic Strain Hardening for FCC Metals," *Phil. Mag.*, 12: 1229–48 (1965).

38. C. F. Feltner and C. Laird, "Cyclic Stress-Strain Response of F.C.C. Metals and Alloys-II Dislocation Structure and Mechanisms," *Acta Metall.* 15: 1633–53 (1967).

39. M. F. Ashby and R. A. Verrall, "Diffusion-Accommodated Flow and Superplasticity," *Acta Metall.*, 21: 149–163 (1973).

40. M. F. Ashby, "A First Report on Deformation-Mechanism Maps," *Acta Metall.*, 20: 887–96 (1972).

41. R. E. Reed-Hill, W. R. Cribb, and S. N. Monteiro, "Concerning the Analysis of Tensile Stress-Strain Data Using Log $d\sigma/d\varepsilon_T$ Versus Log σ Diagrams," *Metall. Trans.* 4: 2665–67 (1973).

42. G. Zankl, *Z. Naturforsch.* 18a: 795–809 (1963).

43. K. C. Liu, *Yield Surfaces and the Elastic-Plastic Behavior of Type 304 Stainless Steel at Room Temperature*, ORNL/TM-5421 (to be published).

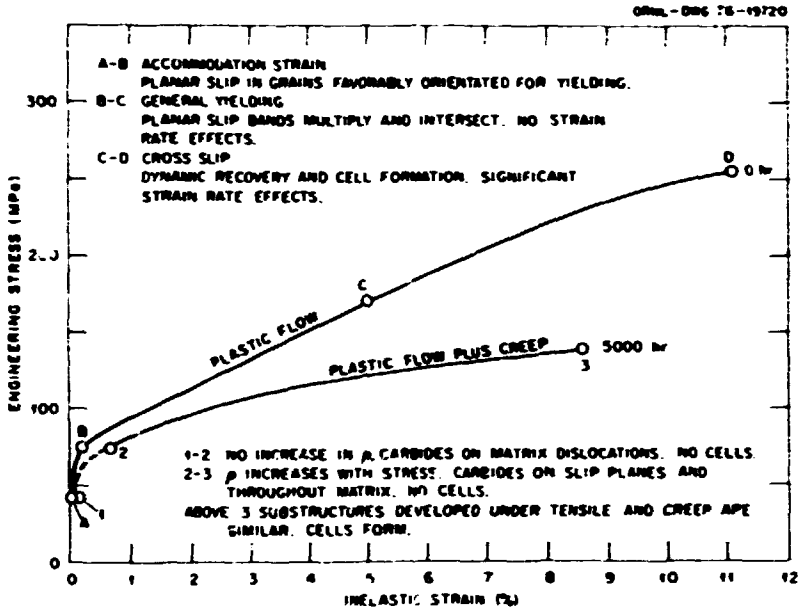

Fig. 40. Substructures developed in different regions of the isochronous stress-strain curves at 593°C for 0 and 5000 hr.

strain bursts.[44] It is well established by Stiechen and other researchers[45,46,19] that flow stress is relatively independent of strain rate, but possibly flow stress for type 304 stainless steel is inversely related to strain rate due to dynamic strain-aging phenomena. In other words, plastic flow and hardening are essentially athermal for conditions of interest to most LMFBR plastic-flow problems.[19] Any unified deformation model must account for this athermal condition. In contrast, many of the glide deformation models proposed in recent years[10,11] make use of thermal-stress activation-analysis principles[10,11] such as those developed from the work of Seeger[47] and others.[48,49] These models will have to be modified to account for observed behavior.

The conditions under which planar slip gives way to cross slip (point C) have not been established for our material, and work on this subject should be initiated soon. We can expect, however, that as flow stress increases, and the plastic strain accumulates under either monotonic or cyclic-strain modes, significant dislocation interaction and tangling will develop at intersections of active slip planes. Cross-slip processes will be activated and dynamic-recovery processes will become significant. This change leads to cell and subgrain formation (C to D). It is consistently observed that as both stress and strain increase conditions are

---

44. D. Fahr, *Analysis of Stress-Strain Behavior of Type 316 Stainless Steel*, ORNL-TM-4292, Oak Ridge National Laboratory (November 1973).

45. J. M. Steichen, "Mathematical Description of the Elevated Temperature Flow Behavior of Type 304 Stainless Steel at High Strain Rates," *J. Test. Eval.*, 1: 520 (1973).

46. J. P. Hammond and V. K. Sikka, *Heat-to-Heat Variations of Total Strain (to 5%) at Discrete Stress Levels in Types 316 and 304 Stainless Steel from 24 to 316°C*, ORNL/NUREG/TM-57, Oak Ridge National Laboratory, (November 1976), p. 30.

47. A. Seeger, "The Mechanism of Glide and Work Hardening in FCC and HCP Metals," pp. 243 - 349 in *Dislocations and Mechanical Properties of Crystals*, ed., J. C. Fisher, Wiley and Sons, New York, 1957.

48. H. Conrad, "Thermally Activated Deformation of Metals," *J. Metals*, 16: 582 - 88 (1964).

49. R. W. Armstrong, "Thermal Activation Strain Rate Analysis (TASRA) for Polycrystalline Metals," pp. 306 - 13 in *Defect Interactions in Solids*, eds. K. I. Vasu et al., Indian Institute of Science, Bangalore, 1972.

approached where strain-rate behavior under tensile conditions conforms to the expectations based on thermal-stress activation principles. The glide processes for plasticity and creep become one and the same. Moteff and coworkers[24,50] have established that the substructures developed in high-stress tensile and creep tests are very similar.

Different ranges can also be identified in the 5000 hr isochronous curve at 593°C (curve 1-2-3 in Fig. 40). In the stress range corresponding to the accommodation strain range, the creep strains are low; no significant increase in the dislocation density is observed, and no cells are developed. The major modification in the substructure due to creep exposure is the precipitation of carbides on some dislocations. This precipitation influences the plastic-flow stress and creep behavior. In the stress range where planar slip occurs under plastic conditions (segment 2-3 in Fig. 40), the creep strains after 5000 hr become equivalent to or larger than the plastic loading strains, ρ tends to increase with stress, and again no cells form. Data available at 121 and 172 MPa suggest that the total dislocation density does not change greatly as a consequence of the accumulated creep strain. If this observation is true, further studies of the transition of substructure in the early stages of creep could be of benefit in understanding creep-plasticity interactions. Clearly, cyclic loading must also be included in such an activity. At stresses where cross slip and dynamic recovery are significant (beyond point 3), plasticity-produced and creep-produced substructures are indistinguishable. Constitutive equations could be based on a rate type of approach.

Returning to low stresses, we now consider how the substructure developed under plastic strain or creep influences subsequent creep behavior. A logical focal point for such a consideration is the often used Orowan expression:

$$\dot{\epsilon} = \mathbf{b}\rho_m \mathbf{v} . \tag{1}$$

where $\dot{\epsilon}$ is the strain rate, $\mathbf{b}$ is the Burgers vector, ρ_m is the mobile dislocation density, and v is the average dislocation velocity. Clearly, if the introduction of plastic or creep strain increases ρ_m, the creep rate will increase, assuming for the moment that the dislocation velocity is not influenced by the value of ρ_m. Unfortunately ρ_m is not synonomous with the dislocation density reported in Table 1, but is probably a function of the applied stress level, σ_a. As pointed out by McLean[51] and others,[52] a mobile dislocation at a high stress might not be mobile at a low stress. Odén et al.[17] define a mobile dislocation as one which has a length, l, so that

$$l \geq l_n = \alpha G\mathbf{b}/\sigma . \tag{2}$$

where l_n is a critical length given by the right-hand side of the equation, G is the shear modulus, σ is the stress on the dislocation, $\mathbf{b}$ is the Burgers vector, and α is a material constant. It has been shown by Odén et al.[17] that creep strains produce large increases in the total dislocation density, but significant decreases in the mobile dislocation density. Plastic strains are also known to increase the total dislocation density, and by implication the mobile dislocation density as defined by Odén et al.[17] would decrease.

---

50. K. D. Challenger and J. Moteff, "Quantitative Characterization of the Substructure of AISI 316 Stainless Steel Resulting from Creep," *Metall. Trans.* 4: 749–55 (1973).

51. D. McLean, "The Physics of High Temperature Creep in Metals," *Rep. Progress Physics*, 29: 1–33 (1966).

52. A. S. Argon, "A Statistical Theory for Easy Glide II," *Physics of Strength and Plasticity*, MIT Press, Cambridge, Mass., 1969, 217–53.

Our data suggest a different trend, however. For example, ρ does not seem to change greatly during creep, and plasticity does not seem to produce much hardening. In fact, some of our unpublished data show that small plastic strains can actually accelerate creep for a short time.

It is clear that the mobile dislocation density, ρ_m, should be greatly influenced by the precipitation of the $M_{23}C_6$ carbide. The matrix carbide does not precipitate under very short-time plasticity situations; hence, the strengthening when creep commences is primarily associated with the changes in the dislocation configuration. Eventually, when the matrix carbide does develop, the fine precipitates observed at temperatures in the 538 to 621°C range immobilize by pinning many of the dislocations having large values for L. Further, the carbides appear to stabilize a fine dislocation network, as discussed by Hopkin and Taylor,[53] and thus produce strengthening for both creep and plasticity situations. To make matters more confusing, however, there seems to be some evidence that the large blocky precipitates which form at 650°C and above can act as dislocation sources under thermal cycling conditions.[54]

The mobile dislocation velocity term, v, in the Orowan equation is thought to depend on temperature, stress, activation volume, and total dislocation density. The specific formulation for v depends on the details of the deformation mechanism,[25] however, which we have not identified for our material. Velocity should increase with temperature and stress and decrease with the activation volume and total dislocation density. Depending upon the specific model, the substructure studies of the type performed here may be extended to provide data to estimate v. A closer coupling between experimental and analytical work would be required to produce anything truly useful, however. Because creep is a slow, more or less continuous process, it is easy to imagine dislocations moving at some average velocity and contributing to the total deformation. However, in the recent model developed by Lagneborg,[16] dislocations glide "rapidly" between arrested positions, and in this sense, deformation by creep and plasticity could be very similar. Without a sound knowledge of the precise mechanism it cannot be shown that the same constitutive relationships should apply to both loading situations. From an experimental viewpoint, the separation of creep and plasticity for low stresses seems justified.

Among the most often demonstrated correlations between substructural parameters and mechanical variables are the relations between stress and dislocation density and stress and subgrain (or cell) size. In Fig. 41, the square root of the dislocation density, $\sqrt{\rho}$, is plotted against the modulus-compensated true stress (σ/G), using data from Table 1. Also included in the figure is a dashed trend line based on specimens tested at higher temperatures.[50] The line conforms to the observation that $\sqrt{\rho}$ is inversely proportional to the stress under steady-state creep conditions. It is interesting to note that data from Table 1 generally fall above the line, meaning that the dislocation densities are too high. The data in Table 1 have been obtained from specimens tested into different creep stages but also at temperatures generally below those used to develop the line. The reasons for this difference have not been determined, but it does seem possible that the relation between $\sqrt{\rho}$ and (σ/G) could be temperature sensitive below 650°C. If so, then there are some interesting implications. These come about if we accept the concept that an internal stress σ_i exists so that

$$\sigma_i = \alpha G B \sqrt{\rho} \qquad (3)$$

---

53. L. M. T. Hopkin and L. H. Taylor, "Creep Properties of Cr-Ni-Mo Austenitic Steel in Relation to Structure," *J. Iron Steel Inst.* 265, 17–27 (1967).

54. S. R. Keown, "Microstructural Changes Occurring During the Creep Deformation of a Simple Austenitic Steel at 600°C," pp. 78–85 in *Creep Strength in Steel and High-Temperature Alloys*, Metals Society, London, 1974.

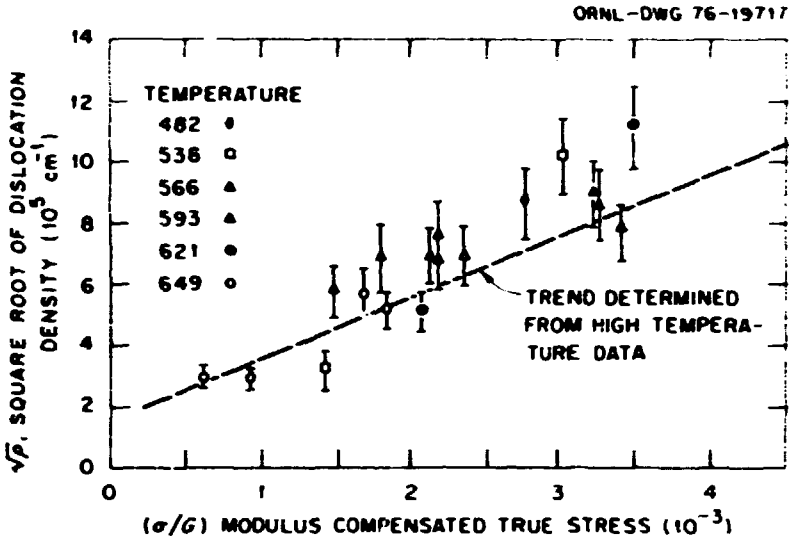

Fig. 41. Square root of dislocation density vs modulus-compensated true stress.

where α is a material constant whose value lies in the range 0.3 to 0.6. Using internal-stress concepts, we assume that the effective stress, σ^*, which produces deformation, is given by

$$\sigma^* = (\sigma_a - \sigma_i) \tag{4}$$

where σ_a is the applied stress. By definition, in Eq. (3), σ_i is proportional to the $\sqrt{\rho}$, and by observation, σ_a is proportional to $\sqrt{\rho}$. Therefore σ_i is proportional to σ_a. This means σ^* is also proportional to σ_a, and the ratio σ^*/σ_a will be a constant. However, if the relation between σ_a and $\sqrt{\rho}$ is temperature sensitive, σ^*/σ_a will also be temperature sensitive, which intuitively seems reasonable. We might expect that at low temperatures (σ^*/σ_a) should be small, and at high temperatures (σ^*/σ_a) should be large. Techniques for determining this ratio have been developed by Cuddy,[55] Nix and Adquist,[56] and Wilshire and coworkers.[57,58] We have also planned experimental work in this area.

The steady-state creep rate, $\dot{\epsilon}_s$, is thought by some investigators to depend on σ^* according to the power law. Thus,

$$\dot{\epsilon}_s = K(\sigma^*)^n = K(\sigma_a - \sigma_i)^n \tag{5}$$

where K and n are material constants. If a relationship such as that shown in Eq. (5) really exists for creep, then an understanding of how σ_i relates to composition and substructure can be of considerable value in

55. L. J. Cuddy and J. C. Roley, "The Effect of Internal Stress on the Activation Parameters for Creep of Fe-Ni Alloys," *Acta Metall.*, 21: 427–33 (1973).

56. C. N. Ahlquist and W. D. Nix, "A Technique for Measuring Mean Internal Stress During High-Temperature Creep," *Scripta Met.*, 3: 679–82 (1969).

57. K. R. Williams and B. Wilshire, "On the Stress- and Temperature-Dependence of Creep of Nimonic 80 A," *Met. Sci. J.* 7: 176–79 (1973).

58. P. W. Davies et al., "Stress-Change Experiments During High-Temperature Creep of Copper, Iron, and Zinc," *Met. Sci. J.* 7: 87–92 (1973).

understanding hardening and recovery concepts. In addition to a simple assessment of the total dislocation line density, more detailed characterization of the dislocation network character can be of value, especially if the study is performed in conjunction with variable-load tests which involve recovery periods,[17] and reversed stresses as examined by Gittus.[59]

The other microstructural correlation mentioned earlier involves the dependence of the cell or subgrain size, λ, on stress. According to the data of Challenger and Moteff[34,50] and Sikka et al.,[60] austenitic stainless steels follow one of two trends. Under high-stress monotonic and cyclic conditions where cells form, λ is inversely proportional to the square of the stress. At low stresses, λ is inversely proportional to stress. A comparison of data reported in Table 1 to a previously determined relationship[50] is shown in Fig. 42. These new data follow the low-stress (linear) trend, but tend to exhibit smaller cell and subgrain sizes than expected from earlier work.

Robinson and Sherby[61] have suggested that the subgrain size plays a significant role in the creep process. They have developed an expression for the steady-state creep rate in which subgrain size is explicitly included:

$$\dot{\epsilon}_s = K(T)\lambda^3 \left(\frac{\sigma}{M}\right)^7 \tag{6}$$

where M is the modulus, and K is a temperature-dependent constant. Since the low-stress data for our material are inversely proportional to λ, the apparent exponent on the stress term should be reduced to 4

59. J. H. Gittus, "The Mechanical Equation of States: Dislocation Creep Due to Stresses Varying in Magnitude and Direction," *Philosophical Magazine*, 24, 1423–40 (1971).

60. V. K. Sikka, H. Nahm, and J. Moteff, "Some Aspects of Subboundary and Mobile Dislocations During High-Temperature Creep of AISI 316 and 304 Stainless Steel," *Mater. Sci. Eng.*, 20: 55–62 (1975).

61. S. L. Robinson, C. M. Young, and O. D. Sherby, "Constant Structure Creep Tests and the Influence of Subgrain Size on Creep," *J. Mater. Sci.*, 9: 341–43 (1974).

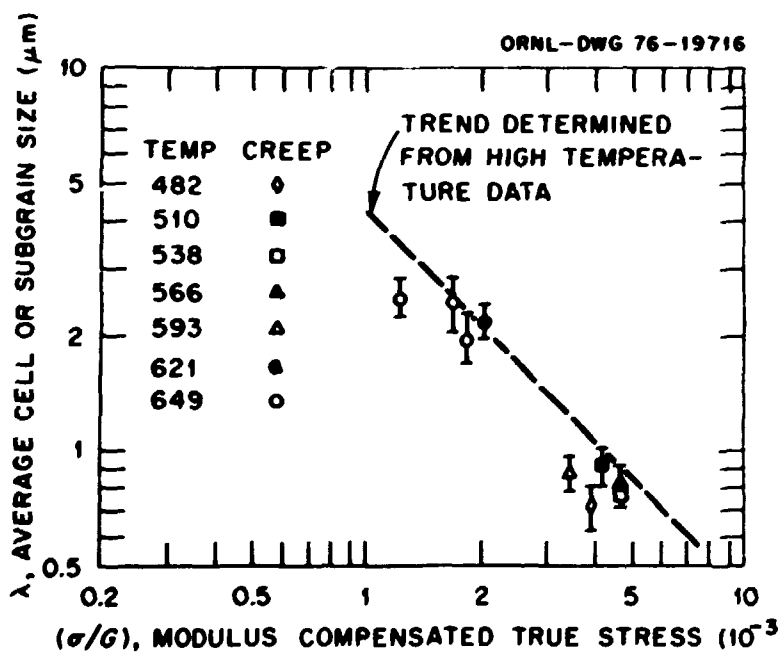

Fig. 42. Average cell or subgrain size vs modulus-compensated true stress.

for conditions under which subgrains form. However, at other temperatures, such as 593 and 538 C, the stress exponent should remain at 7, since λ is constant and equivalent to the grain size.

The formation of subgrains is also known to have a significant influence on the yield strength, σ_y, especially at lower temperatures where the Hall-Petch relationship usually holds. Additional studies by Young and Sherby[62] and Miller and Sherby[63] show that the following relation holds:

$$\sigma_y^2 = \sigma_o^2 + k^2 \lambda^{-2m} \tag{7}$$

where σ_o, k, and m are material constants. The applicability of this relationship to intermediate temperatures should be examined since it could be of value in understanding the nature of creep-plasticity interactions.

The $M_{23}C_6$ carbide which precipitates in type 304 stainless steel can affect mechanical behavior and constitutive equation development in several ways. Carbon in solution is known to be a potent strengthener in regard to plastic flow strength.[23,64] Hence, depletion of this element could produce loss in strength. In fact, the relatively fine dispersion which occurs at temperatures in the range of 500 to 650 C results in strengthening rather than weakening. Sikka et al.[23] have shown that the time at which aging begins to increase the flow stress corresponds to the time required for the precipitation of matrix carbides. Etienne et al.[65] have made similar observations for cyclic flow behavior. On the other hand, if carbon really plays a role in the strain-aging behavior, then the depletion of carbon could influence the flow-stress vs strain-rate response in the temperature range of 350 to 650°C. It must be recognized that the strain-aging behavior probably involves solute elements as well as interstitials; therefore, strain aging should still be present after aging. Sikka et al.[23] find that aging produces higher creep rates in type 304 stainless steel, a similar response has been observed in other steels.[66,67,26] This seems to be inconsistent with the observation that the precipitate stabilizes a fine dislocation substructure in the temperature range of 500 to 625 C which results in an increase in creep strength. The key to the explanation is probably associated with the fact that the carbide-precipitation characteristics are different under highly stressed conditions than under simple aging. It is well established that the kinetics of the precipitation process are influenced by the presence of stress and strain. Etienne et al.[65] have shown this, using a material (heat L) which is very similar in composition and strength to the material we have studied. We have replotted their time-temperature transformation diagrams for low-stress aging in Figs. 43 and 44. Figure 43 shows the precipitation kinetics of matrix carbides with and without stress. The data confirm that high stresses accelerate both the start and the growth rate of the matrix carbides, especially at the higher temperatures. Our investigations reveal that the carbides often delineate the planar-slip traces produced on plastic loading after the dislocations have climbed or cross slipped out of the planes and developed cellular configurations. Figure 44 shows the

---

62. C. M. Young and O. D. Sherby, "Subgrain Formation and Subgrain Boundary Strengthening in Iron-Based Materials," *J. Iron and Steel Inst.*, 211: 640–47 (1973).

63. A. K. Miller and O. D. Sherby, "On Subgrain Strengthening at High and Low Temperatures," *Scripta Met.*, 10: 311–17 (1976).

64. K. Natesan, T. F. Kassner, and C. Y. Cu, "Effect of Sodium on Mechanical Properties and Friction-Wear Behavior of LMFBR Materials," *Reactor Technol.* 15: 244 (Winter 1972/1973).

65. C. F. Etienne, W. Dortland, and H. B. Zeedijk, "On the Capability of Austenitic Stainless Steel to Withstand Cyclic Deformation During Service at Elevated Temperature," paper presented at Int. Conf. Creep and Fatigue in Elevated Temperature Applications, Philadelphia, September 1973, and United Kingdom, Sheffield, April 1974.

66. J. T. Barnby, "Effect of Strain Aging on Creep of an AISI 316 Austenitic Stainless Steel," *J. Iron and Steel Inst.*, 204: 23–27 (1966).

67. F. F. Asbury and G. Willoughby, "Aging and Creep Behavior of a Cr-Ni-Mn Austenitic Stainless Steel," pp. 144–51 in *Creep Strength in Steel and High-Temperature Alloys*, Metals Society, London, 1974.

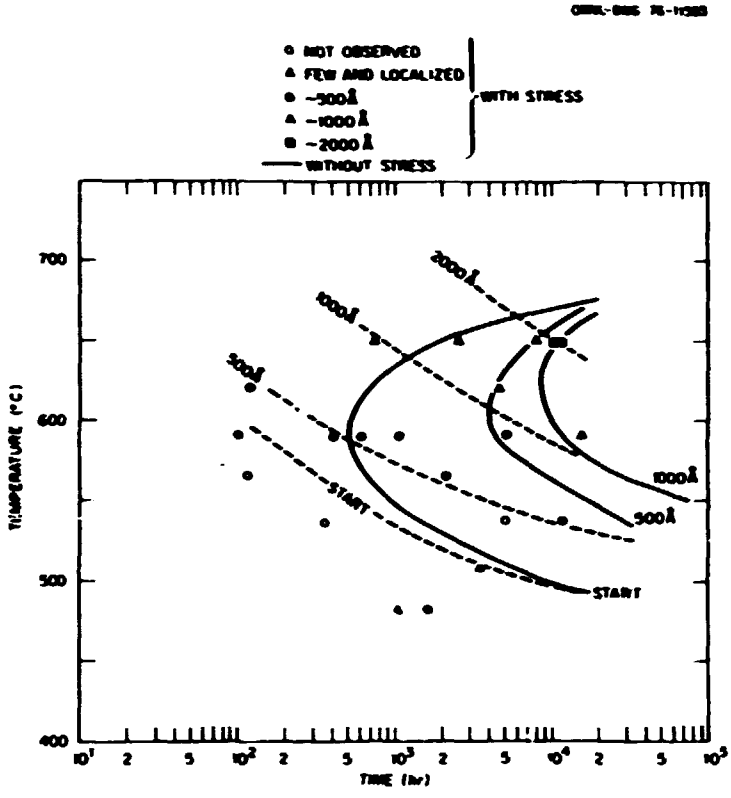

Fig. 43. Influence of stress on the precipitation kinetics of $M_{23}C_6$ within the matrix of type 304 stainless steel.

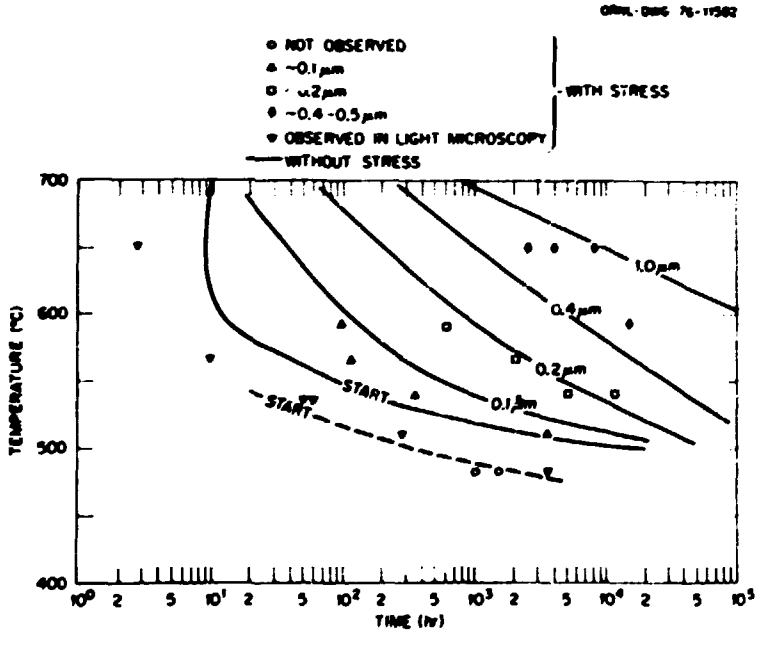

Fig. 44. Influence of stress on the precipitation kinetics of $M_{23}C_6$ within the grain boundaries of type 304 stainless steel.

precipitation kinetics of grain boundary carbides. In this case, the stress or strain seems t accelerate the start of the precipitation, especially at lower temperatures. The influence of grain boundary precipitates on the yield and flow behavior of our material has not been emphasized in this report. Actually, grain boundary carbides could play a significant role. At high temperatures the carbides precipitate quickly, and under some conditions denuding of carbon and chromium develops in zones on either side of the grain boundary.[23,68] This relatively weak material could exhibit significantly different flow characteristics than the matrix away from the boundary does, and this possibility complicates efforts to describe hardening behavior. Under lower stress conditions, Keown[54] observed that grain boundary carbides alter the dislocation's emitting or absorbing the characteristics of the boundary.[54] Further, the very presence of the precipitate complicates efforts to estimate the grain boundary diffusion contribution to creep, which has an impact on the position of the different fields on the Ashby deformation map and thus compromises the usefulness of the approach.

In all probability the carbide precipitation, especially on the grain boundaries, has an enormous influence on the rupture life and ductility. We have accumulated a significant body of data bearing on this subject for type 304 stainless steel. These data are currently being evaluated. As an example, in one study,[69] the power law has been used to represent isothermal rupture data in the temperature range of 482 to 816°C:

$$1/t_r = (\sigma/A)^{n_r} \tag{8}$$

where A and n_r are temperature-dependent constants which are determined by least squares. Plots for A and n_r against temperature are shown in Fig. 45, and it appears that n_r increases with increasing temperature to nearly 600°C then decreases precipitously. The peak value of n_r occurs where the precipitate-dislocation interaction is most prominent.

68. R. Stickler and A. Vinckier, "Morphology of Grain-Boundary Carbides and Its Influence on Intergranular Corrosion of 304 Stainless Steel," *Trans. Amer. Soc. Metals* 54: 362 (1961).

69. R. W. Swindeman, "Creep-Rupture Correlations for Type 304 Stainless Steel (heat 9T2796)," *Symp. Struct. Mater. Elevated-Temperature in Nucl. Power Generation Service*, ed. A. O. Schaefer, MPC-1: 1–30, 1975.

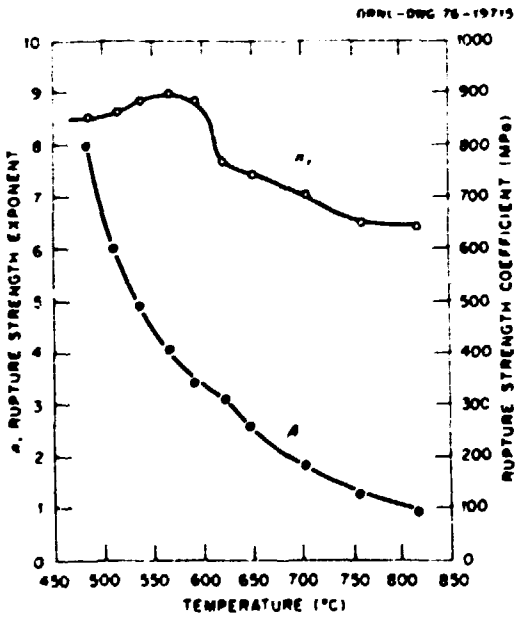

Fig. 45. Variation of A and n_r with temperature.

CONCLUSIONS

1. At stresses which produce less than 1% accumulated inelastic strain in 10,000 hr or less, the observed dislocation densities are close to the starting value (10^9 cm^{-2}). No evidence of cell formation exists. The major alteration of substructure is the precipitation of $M_{23}C_6$ on grain boundaries, twin boundaries, and on some dislocations. This precipitation is observed in the temperature range 538 to 649°C.

2. At stresses which produce greater than 1% accumulated inelastic strain in 10,000 hr or less, the observed dislocation densities and substructures depend on the temperature and stress level.

3. At stresses in the range 69 to 172 MPa, and for temperatures in the range 482 to 593°C, the observed dislocation density tends to increase with increasing stresses. To a first approximation the density increases with the square of the stress. Dislocation densities are greater than expected based on studies at comparable stresses and higher temperatures, however. No evidence of cell formation exists; rather, dislocations are arranged in fairly fine networks and sometimes in dense tangles, which appear to be stabilized by fine precipitates.

4. At stresses in the range of 69 to 172 MPA, and for temperatures above 593°C, the observed dislocation densities increase, approximately with the square of the stress. The cell size is inversely proportional to the stress. The cells are well developed and could be classified as a mixed configuration or even as subgrains in some cases.

5. At stresses above 172 MPa, and for temperatures in the range 482 to 649°C, dislocation densities are very high and difficult to evaluate. Cells develop whose walls consist of dislocation tangles. The cell size is inversely proportional to the stress, but tends to be finer than the cell size determined at similar stresses but at higher temperatures.

6. Substructures developed under cyclic plasticity conditions vary in character with the temperature. At 427 and 482°C, dislocations are often arranged in primitive cells or bundles. The dislocation densities fall within the scatter band exhibited by monotonic data. Similarly, the cell sizes fall within the scatter band for monotonic data. At 649°C, the substructure is somewhat variable, exhibiting some regions of primitive cells and other regions of fairly well-defined cells. The dislocation densities and cell sizes are in agreement with the trends established from high-temperature data.

7. Exposure to creep conditions accelerates the growth of $M_{23}C_6$ carbides in the matrix, especially at higher temperatures. It also accelerates the start of precipitation of grain boundary carbides at all temperatures.

8. The substructural data developed here do not refute the current constitutive equations which treat plasticity and creep strain separately with respect to yield, flow, and hardening behavior. There is an urgent need, however, to perform more studies on tensile and creep tested specimens in the early stages of hardening. More study of substructures produced under cyclic-plasticity and cyclic-creep conditions are also needed.

ACKNOWLEDGMENTS

The authors thank H. E. McCoy, Jr., R. L. King, C. R. Brinkman, and G. M. Slaughter for review and helpful discussions. Assisting in the report preparation were Carolyn Strizak and the Technical Publications Department. The unnumbered transmission-electron micrographs in this report were provided by the University of Cincinnati in conjunction with their subcontract.